INS-NUMA-38

Japanese Facilities for HIF Accelerator Development

T. Katayama, A. Noda and Y. Hirao

June, 1982

STUDY GROUP OF NUMATRON AND
HIGH-ENERGY HEAVY-ION PHYSICS
INSTITUTE FOR NUCLEAR STUDY
UNIVERSITY OF TOKYO
Midori-Cho 3-2-1, Tanashi-Shi,
Tokyo 188, Japan

INS-NUMA-38
June 1982

Japanese Facilities for HIF Accelerator Development

T. Katayama, A. Noda and Y. Hirao

Institute for Nuclear Study, University of Tokyo

3-2-1 Midori-cho, Tanashi-shi, Tokyo, Japan

Abstract

Ion storage ring named TARN has been successfully operated at INS, which stores the low velocity ions ($\sim$ 7 MeV/u) in the betatron and synchrotron phase spaces by the amount of a few hundred turns. The operation results of the ring are described as well as the possible use of the ring for the study of beam dynamics in the storage ring of HIF scenario.

Design outlines of NUMATRON, high energy heavy ion accelerator project in Japan, are given especially from the point of view of its usefulness for HIF accelerator study.

Presented at the Symposium on Accelerator Aspects of Heavy Ion Fusion, March, 1982, at GSI, Darmstadt.

1. Introduction

In Japan, a working group was organized by researchers in various scientific fields in order to study on the design of heavy-ion beam fusion-power generation system, in 1980.[1,2,3] Main institutes which are collaborating on this subject with each other, are the Institute of Plasma Physics of Nagoya University (IPP), the Institute of Laser Engineering of Osaka University (ILE), the National Laboratory for High Energy Physics (KEK) and the Institute for Nuclear Study of University of Tokyo (INS). The former two participate mainly on the design of pellet and reactor system, while the latter two on the study of heavy ion accelerator system. The INS has taken a major part of the accelerator design as they have experienced in the accelerator physics of heavy ion beam related with the high-energy heavy-ion accelerator project (NUMATRON).

It is well recognized that experimental studies on the beam dynamics are quite important as well as the theoretical investigations on the HIF scenario. Acceleration in low-velocity linac and stacking and bunching in rings are key issues in the driver system consisting of RF linacs and storage rings as well as bunching and focusing in the final beam lines. The existing machines are, however, designed and used for studies of nuclear and particle physics and their specifications do not necessarily satisfy the required conditions for HIF accelerator studies. Considering such circumstances of accelerators in the world, heavy ion accelerator projects such as SIS, VENUS and NUMATRON are strongly expected to be authorized as early as possible from the point

of views not only of nuclear physics but also of HIF studies. They would bring about many experimental results, being suggestive and useful for conceptual design of HIF accelerator.

Even in the existing accelerators, however, it is possible to study experimentally on the limited subjects regarding the beam dynamics in HIF scenario. In Japan, we are now performing experiments of low energy beam stacking in a storage ring named TARN and of acceleration in a low velocity region with a RFQ linac named LITL, which have been constructed as a part of preparatory works on NUMATRON project. Experimental results as well as some possible uses for HIF study of TARN are described in the section 2, while the activity in the RFQ study is presented in a separate paper to this symposium.

The new version of the NUMATRON consists of high current linac and two synchrotron rings which can provide various ion beams from hydrogen to uranium of energies up to several GeV per nucleon and promote the heavy ion science such as nuclear physics, atomic physics and medical biology. The accelerator capability is also quite useful to perform fundamental investigations for HIF study. In the section 3, some possible uses of NUMATRON for HIF accelerator and target physics are described.

2. TARN — Test Accumulation Ring for NUMATRON —

A small ion storage ring, TARN has been constructed at INS for developing exclusively accelerator technology related to NUMATRON project. It has been aimed at storing low energy 7 MeV/u ion beams both in the betatron and synchrotron phase spaces from the INS-SF cyclotron.

The layout and overview of the ring are shown in Figs. 1 and 2 and main parameters are given in Table 1.

By use of this ring, it is possible to study experimentally on the limited subjects regarding the beam dynamics in HIF scenario. In the following sections, experimental results of TARN are described as well as some possible uses of the ring for the HIF studies.

2-1. Beam stacking experiments in TARN

After the first success of beam injection in the TARN, July of 1979, we have made beam stacking experiments and have obtained the results which are in close agreement with theoretical calculations. They are summarized as follows.

a) Beams are transported from the cyclotron and are stacked in the betatron phase space of TARN by the amount of $\sim$ 20 turns. (Fig. 3)

b) They are debunched and adiabatically captured by the RF field and are moved to the top of stacking orbit which is 8 cm apart from the injection orbit. The capture efficiency is $\sim$ 70 % through this process. (Fig. 4)

C) RF stackings are performed with the repetition rate of 33 Hz and the beam intensity in the ring is increased linearly up to the RF stacking number of around 15. When stackings are performed more than $\sim$ 15 times, the stacking efficiency is decreased. (Fig. 5)

d) Profiles of multiturn injected and RF stacked beams are measured with destructive beam profile monitors. The betatron amplitude of multiturn injected beam is 17 mm at the centre of the straight section

while the 20 times RF stacked beam occupy the spatial range of 5 cm. (Fig. 6) The momentum spread of RF stacked beam is estimated at 2.2 % which corresponds to $\sim$ 20 times larger than the momentum spread $\sim$ 0.1 % of injected beam.

e) Over all stacking number is a few hundred turns.

Details of the ring can be found in the references,[4,5] however fundamental ideas of beam accumulation method are shortly described here.

Magnetic focusing system of the ring are eight bending magnets and sixteen quadrupole magnets with a lattice structure of FODO type. Additionally twelve sextupole magnets of two sets are installed for chromaticity corrections. The mean radius is 5.06 m while the bending radius of central orbit is 1.333 m. Eight straight sections, each of which is 1.80 m length, are served for various instruments of beam injection, stacking and beam diagnostic systems. Beams are transported from the cyclotron to the ring by the distance of $\sim$ 40 m and the momentum is analyzed to $\sim 1 \times 10^{-3}$ through the line. A kicker magnet located in the transport line, shapes the beam pulse width to $\sim$ 80 μsec suitable for multiturn injection. By the use of an electrostatic inflector and two bump magnets, beams are injected in the betatron phase spaces with the area of 103 π mm·mrad. Horizontal beam emittance at the injection point of the ring is assumed at 5 π mm·mrad and the net circulating current will be 18 turns. In this multiturn injection method, loss rate of the beam is calculated at 45 %.

Multiturn injected beam is debunched at $\sim$ 250 μs after the injection

due to its intrinsic momentum spread. Then the RF voltage is increased from zero to 77 V adiabatically in order to capture the coasting beam in the separatrix, of which the area is equal to the beam longitudinal phase space area, 100 keV.rad. In this capturing process, RF frequency is kept constant at 8.012 MHz, seven times the revolution frequency of particles on the injection orbit and hence the synchronous phase angle ϕ_s is 0 degrees. Period of phase oscillation is 0.45 ms at the end point of capture process and the period for increasing the voltage from zero to 77 Volt is chosen as 0.5 ms. Computer calculation shows that the rising period of nearly phase oscillation period can achieve the highest capture efficiency ($\sim$ 80 %), whereas too shorter or longer period fail to trap the beam in the separatrix. In Fig. 7 the functions of RF voltage and frequency are illustrated and parameters of RF stacking dynamics are given in Table 2. After the capture process (Region I), synchronous phase is increased from 0° to 15° (Region II), kept constant as 15° (Region III) and finally changed back to 0° (Region IV). Through the whole process, separatrix area is kept constant at 100 keV·rad in order to prevent the dilution of beam in the longitudinal phase space.

The RF stacking is repeated at 33 Hz and the beam intensity increases linearly up to the stack number of 15, while it shows the saturation at more stackings (Fig. 5). From the experimental data of beam profiles (Fig. 6), an amplitude of betatron oscillation x_β is measured at 17 mm and the emittance of the multiturn injected beam is deduced at 87 π mm·mrad, when the emittance of injected beam is 3.8 π mm·mrad. The momentum spread of the stacked beam can be estimated by

measuring the spatial spread. Subtracting the injected beam width from the whole beam width, one gets 35 mm at the stacking number of 15. As the dispersion function is 1.6 m at the straight section, the resultant momentum spread is 2.2 %. The momentum spread of the injected beam is 0.1 % and the dilution factor in the longitudinal phase space is calculated at 1.5.

When the injected beam is moved to the stacking orbit, the working line can be chosen so as to cross the resonances such as integer, half integer and third order resonances, Possible working lines with sextupole magnet excitation are calculated[6] and given in Fig. 8. Experimentally one third of the injected beam is lost during the cross of 1/3 resonances. In Fig. 9 the signals of lost beam are observed (top) by scintillation monitor located inside the vaccum chamber. The lower in the figure shows the RF frequency variation which corresponds to the beam position and working points in the tune diagram.

As the preparatory work for stochastic beam cooling experiment, observation of Schottky signal was performed. Signals from an electrostatic pick up was fed to a low noise preamplifier with a noise figure of 2.5 dB and the output signals are spectrum analyzed.

By use of the averaging function of spectrum analyzer with minicomputers, thermal noise current of preamplifier can be cancelled out. A typical example of the spectrum is shown in Fig. 10 where the number of particle is around 10^8 and 2500 times averaging was performed. Each peak corresponds to the harmonic number of 72 and 73, respectively.

When the signals of delta-type electrostatic pick up are analyzed, on-line tune values can be measured. Typical example of the spectrum is given in Fig. 11 where the spacing of transverse and longitudinal modes Δf is 278 kHz. It is related with the fractional part of tune value q as

$$q = \Delta f / f_0 \quad .$$

From the result, the ν-value at the injection orbit is calculated at 2.245, which is in close agreement with the value 2.241 obtained by an RF knock out method.[6)]

2-2. Further beam experiments at TARN

Following beam experiments are scheduled and preparations are in progress.

a) Resonance crossing experiments.

Integer, parametric and higher order resonances are crossed by sweeping the closed orbit with RF frequency modulation and by the sextupole magnets adjustment. Crossing speeds are arbitrary changed. Beam emittance growth associated with resonance crossing, is measured with beam profile measurement technique.

b) Beam transfer function measurement.

The response of a beam to small transverse and longitudinal RF excitations is analyzed with Fast Fourier Transformer (FFT) which measures a spectrum nearly 100 times faster than the conventional

spectrum analyzer. From the measured spectrum one can get a lot of informations about the beam distributions, wall impedances and also space charge impedances. As is noted in the next section, space charge impecance predominantly determines the stability conditions in the HIF rings and then the impedance measurements in the low energy rings such as TARN are important works.

c) Stochastic beam cooling.

In TARN many pulses are RF stacked in the momentum phase spaces with its spread of 2 % or more and then stochastic momentum cooling is quite useful technique for obtaining the monochromatic heavy ion beams in the ring. Electronic systems with the band width of 100 MHz are prepared, by which the cooling time is expected to be ∿10 seconds. First trial is scheduled at the end of this year.

Besides these scheduled experimental studies, following plans are under discussion.

New injector linac for the light ion beam will be constructed which can accelerate the ion up to the energy of 5 Mev/u with the peak current of 5 mA. RFQ linac will be pre-injector of the linac. Beams are injected from the injector linac in the transverse phase spaces by the multi-turn injection method and the circulating current will be 100 mA. Beam instability experiments will be performed as well as the bunch compression study. In Table 3, bunch compression parameters in TARN are listed.

2-3. Coherent Beam Instability at TARN

a) Transverse Coherent Instability

The transverse resistive wall instabilities are found at various high energy accelerators. In the case of TARN, this instability is anticipated much serious due to rather low beam energy.

The stability condition against the transverse coherent instability is given by the relation:

$$\left| \frac{Z_\perp}{Z_o} \right| < 2F \frac{A}{q^2} \frac{\gamma}{N r_c} \nu \left| (n-\nu)\tilde{\eta} + \nu \right| \frac{\Delta p}{p}$$

where the notation is as follows,

Z_o (=120πΩ) is the impedance of free space, F is a form factor depending upon the shape of momentum distributions, a value of 0.45 is assumed for the present case, which is now being studied by dispersion relation analysis, N is the total number of accumulated ions r_c is the classical radius of such a particle as has a unit atomic mass ($m_o c^2$ = 931.5 MeV) and is equal to $\frac{1}{4\pi\epsilon_o} \cdot \frac{e^2}{m_o c^2} = 1.57 \times 10^{-18}$ m, n is the mode number and the nearest integer greater than ν should be used as this value, $\tilde{\eta}$ is equal to $\frac{1}{\gamma_t^2} - \frac{1}{\gamma^2}$ (γ_t is the transition gamma), $\frac{\Delta p}{p}$ is full width of fractional momentum spread at half height, ν is the number of betatron oscillations per revolution, ν' is equal to $\frac{\partial \nu}{\partial (\frac{\Delta p}{p})}$ and A and q are the mass number and charge state of the accumulated ion, respectively. For the ideal case where the beam and the vaccum chamber have constant circular cross sections, transverse coupling impedance $Z_\perp$ (Ω/m) is given by the formula:

$$Z_{\perp} = iRZ_o \left[\frac{1}{\beta^2\gamma^2} \left(\frac{1}{a^2} - \frac{1}{b^2} \right) - (1+i) \frac{\delta}{b^3} \right]$$

where R is the mean radius of the machine and a and b are the radii of the beam and vacuum chamber, respectively and δ is the skin depth of the chamber wall.

For the case of TARN, where β of the circulating beam is low ($\sim$0.121), the transverse coupling impedance is rather large. Then the intensity limit of the transverse coherent instability is estimated at 6×10^8 ions/pulse for N^{5+} without sextupole correction. For α particle and proton with the same kinetic energy, this limit is $\sim 1 \times 10^9$. At the recent experiment of RF stacking, sextupole magnets are excited to controle ν' to be around -2 and for this case the stability limit is 2.8×10^9 particles/pulse, which is thought slightly higher compared with the present accumulated beam intensity. However the above treatment is based on rather ideal case (circular beam and circular beam pipe) and in reality there exist discontinuity of cross section of vaccum chamber and ferrite loaded bump magnets, which seem to raise the coupling impedance. So investigations of beam behaviour in vertical direction are strongly needed together with the increase of beam intensity from the SF cyclotron, which might clarify the relation of threshold current and the tune spread of the accumulated beam. In fact, if an injector linac which can provide 5 MeV/u ions with the peak intensity of 5 mA, the instability limit is largely exceeded.

If we assume the fractional momentum spread to be 3×10^{-3}, the instability limit is 1.1×10^{9} and 6.7×10^{9} for ν' of -0.5 and -6, respectively, while the number of accumulated beam is estimated to be 5×10^{11} when the multi-turn injection is applied. The e-folding growth rate of the instability is calculated at 13.3 msec when the above intensity is accumulated.

b) Longitudinal Instability

Stability limit of longitudinal coherent instability is given by Keil-Schnell criterion:

$$\left| \frac{Z_{11}}{n} \right| \leq F \frac{Am_o c^2 \beta^2 \gamma |\eta|}{q^2 e I_o} \left(\frac{\Delta p}{p} \right)^2$$

where I_o is the particle current (electric current divided by the charge state) and Z_{11} is the longitudinal coupling impedance and other notations are the same as the transverse case.

For the operation condition so far tried, where RF stacking is applied together with the multi-turn injection, $\frac{\Delta p}{p}$ amounts to 2.47 % and the instability limit is calculated at 4.5×10^{12}. This value is much higher compared with the present intensity of the accumulated beam using the cyclotron as an injector.

When the new injector is used, the beam intensity can be raised up to 5×10^{11} without RF stacking. In this case the fractional momentum spread is limited rather small ($\sim 3 \times 10^{-3}$) and the threshold intensity where the instability occurs, is decreased to $\sim 7 \times 10^{10}$ particles. So the ratio of the accumulating current to the threshold current of

the instability, becomes about 7, which is close to the case of Heavy Ion Fusion driver and the experimental study would aid the HIF driver design.

In connection with longitudinal impedance, we should remark that the space charge term predominantly determines the absolute value of the impedance in the case of TARN and HIF storage rings, whereas the resistive wall impedance is leading term in the high energy rings such as CPS. The comparisons between these accelerators are given in Table 4, Which is originally given by D. Möhl at the previous workshop at LBL.[7] As is clear in the Table, longitudinal impedance measurement at the low energy ion storage rings are quite important subjects for HIF accelerator study.

3. HIF Studies with NUMATRON

NUMATRON consists of high current linac and two synchrotrons which can provide various ion beams from hydrogen to uranium of energies up to several GeV/nucleon and promote the heavy ion science such as nuclear physics, atomic physics and medical biology. On the other hand, this machine is designed to be capable of the acceleration and storage of high current heavy ion beams. These accelerator characteristics are also quite useful to perform fundamental investigations for the heavy-ion fusion work.

3-1. Outline of the NUMATRON for HIF Studies

In the NUMATRON project, it is proposed to provide a high intensity

Xe^{8+} beam of 0.5 TW peak power. The layout of accelerator complex is illustrated in Fig. 12.

Each Xe^{1+} beam of 20 mA from two 200 kV Cockcroft-Walton generators is fed to two RFQ linacs, accelerated to 64 keV/u, and funneled into a series of drift tube linacs. Through the linac system, ions are stripped to a Xe^{8+} beam and accelerated to 5 MeV/u. This charge state is preferable for following accumulation process in the ring, because the cross section of charge exchange process is small ($\sim 10^{-18}$ cm^2) due to the closed shell structure of a Xe^{8+} ion, and the beam loss during the accumulation process is reduced. The beam is injected into the first synchrotron by the multiturn injection method (about 15 turns), and accelerated to 28 MeV/u. About 10 pulse from the first ring are accumulated in the second synchrotron by the RF stacking method, and accelerated to 75 MeV/u. The beam is extracted after a bunch compression process and transported to the target. As a beam pulse contains 1×10^{13} ions in a $\pm$ 15 ns pulse width at the target, the total energy is 15.5 kJ and the peak power and current are 0.516 TW and 53.3 particle amperes, respectively.

Properties of the output beam are given in Table 5.

3-2. Ion Source and Injector Linacs

To obtain a high current ion beam, the charge state of injected beam is chosen at a low value. A 40 mA Xe^{1+} beam has been stationally ejected from a Penning discharge, Pierce extraction (PDPE) Source at Argonne National Laboratory. The extraction voltage is 100 kV, and

the normalized emittance is 0.19 π mm·mrad. Using the enriched ^{129}Xe gas a 30 mA ion beam is available. Considering the results of this study, the operation conditions of the ion source and the preacceleration are set as in Table 7.

The linac complex consists of three types of linacs; an RFQ, an interdigital-H and an Alvarez. Though the first two linacs have not been well established, they have advantages in accelerating an ion beam of a low velocity. Therefore it is proposed here to adopt these linacs. The Alvarez linac is preferrable for a high energy beam.

Two RFQ linac are located in parallel at the first stage in a series of linacs, and the beams from the two linacs are funneled into the following linac. In an RFQ, both of the acceleration and the focusing is performed using an rf electric field, and a stronger focusing strength and a shorter cell length are available than a conventional drift tube linac. The operation frequency is determined by the charge to mass ratio and the emittance of the beam, and is set as 12.5 MHz in this design.

Parameters of the RFQ, capable of a high intensity beam, are summarized in Table 7. The phase and the energy spreads of the output beam are respectively 30° and ± 0.97 keV/u ($\Delta T/T$ = ± 1.5 %).

The interdigital-H linacs (IH1, IH2, IH3) operated at 25 MHz follow the RFQ. The structure is simpler than the one of an ordinary off-axis linac (GSI type Widerö̈e linac), and a high shunt impedance is expected to be attained. At this operation frequency the effective shunt impedance is about 150 MΩ/m in a velocity region of β = 1 ∿ 2 %,[8,9]

which is about three thimes higher than that of a Wideröe linac of the π-3π mode.

The beam is accelerated up to 150 keV/u through the IH1, which is operated in the π-3π mode. Through a gas stripper between the IH1 and the IH2 the equilibrium charge state of Xe changes to Xe^{8+}, of which the fraction is about 20 %. The beam energy reaches 300 keV/u through the IH2 in the π-3π mode and 1.6 MeV/u through the IH3 in the π-π mode. The quadrupole magnet sequence in the IH linacs is FFDD.

Two Alvarez linacs operated at 100 MHz accelerate the beam up to 10 MeV/u. The shunt impedance of this type linac exceeds that of an IH linac in the higher energy region $\gtrsim$ 1.6 MeV/u. The quadrupole magnet sequences are FFDD in the first Alvarez and FDFD in the second. The Xe^{8+} beam from the first Alvarez is injected to the first synchrotron skipping the second Alvarez.

Parameters of the whole linacs are listed in Table 8 and Fig. 13. The overall length of the linacs is 124 m, excluding stripper and beam matching sections. The power loss in the linacs is 8.8 MW; 4.6 MW for the beam loading and 4.2 MW for wall loss.

3-3. Synchrotrons

As described previously, the accelerator complex has the two ring synchrotron system, which can provide high-energy heavy ions up to uranium in an energy range from several ten MeV/u to about two GeV/u. For the HIF studies, Xe^{8+} beam of 75 MeV/u is assumed as the most suitable one. In Table 9, various synchrotron parameters of this case

are shown.

The normalized emittance of the Xe^{8+} beam from the injector linac is about 1.0 π mm·mrad, considering the data of 0.2 π mm·mrad at the high intensity xenon source and assumed emittance growth of 5 times in the injector linac, and then the unnormalized emittance at the injection energy of 5 MeV/u is 9.7 π mm·mrad. In the case of 15 turn injection into horizontal phase space, the emittance of injected beam, ε_x, is 218 π mm·mrad, considering a dilution factor of 1.5. In this case, the vertical emittance ε_y, remains at 9.7 mm·mrad. Using the equation

$$N_s = \frac{2\pi\Delta\nu}{Br_o} \left(\frac{A}{q^2} \right) \sqrt{\varepsilon_x \cdot \varepsilon_y}\ \beta^2\gamma^3 \quad ,$$

space charge limit is calculated at 1.05×10^{12} Particles, where B is bunching factor. With a bunching factor of 1, space charge limit is calculated at 1.05×10^{12} ions. The peak current from the linac required to attain this limit is 1.47 pmA, which is smaller than 6.4 pmA designed at the linac system.

The accelerating rf voltage is 21.1 kV/turn, and the voltage to capture a beam with a momentum spread listed in the table are 9.8 kV and 1.1 MV at the first and second rings, respectively.

3-4. Bunch Compression

In the second synchrotron, the beam is accelerated to the energy of 75 MeV/u and is compressed to the pulse width of 112 ns, corresponding to the bunching factor of 10. In the process of bunch compression,

space charge repulsion force becomes quite large and the saw tooth RF voltage should compensate the repulsive lingitudinal force as well as the beam bunching. The longitudinal space charge reactive impedance Z/n is expressed as

$$\frac{Z}{n} = - j\, g\, \frac{Z_o}{2\beta\gamma^2}$$

where g is a geometrical factor ($= 1 + 2\, \ell n\, \frac{b}{a}$) and Z_o is a vacuum impedance. Defining the inductance L as

$$L = - j\, \frac{Z}{n\omega_o}$$

the space charge compensation voltage eV_{sc} is given by

$$eV_{sc} = \pm\, 3N\, qe\, L/2T^2$$

where N is the number of particle per bunch, T is a bunch width in time and q is a charge state of the particle. Numerical values of Z/n, L and eV_{sc} in the present case are tabulated as follows.

$$\frac{Z}{n} = - 851.9\ j\ (\Omega)$$

$$L = - 3.04 \times 10^{-4}\ (H)$$

$$eV_{sc} = \pm\, 930.6\ (KeV)$$

After the compression, the bunch width is shaped as 112 ns and the momentum spread is $\pm 3.85 \times 10^{-2}$.

After the bunch compression, the beam is extracted from the 2nd synchrotron and is transported to the target position, where beam width should be ± 15 ns. The length of drift space for the beam bunching is given by

$$\ell = \frac{\Delta\tau}{\Delta v} v^2$$

where $\Delta\tau$ is a difference of half bunch lengths at the initial and final positions and $\Delta v/v$ is a velocity distribution in the bunch. Through the progress of bunch compression in the beam transport, the space charge force should be compensated as well as in the ring. Assuming the bunch length as L(z) at the position z, the space charge force eE(z) is given by

$$eE(z) = \frac{6qge^2N}{\gamma^2 L^2(z)} \frac{1}{4\pi\varepsilon_o}$$

where γ is a kinematical factor. Assuming that the bunch compression is performed linearly along the path length in the beam line, L(z) is expressed as

$$L(z) = L_i + \frac{L_f - L_i}{\ell} z = a + bz$$

where L_i ans L_f are the bunch lengths at the start and the final positions. Then the total voltage for the space charge compensation is

$$\int_0^{\ell} eE(z)dz = \frac{6gqNmc^2 r_o}{\gamma^2} \int_0^{\ell} \frac{dz}{(a+bz)^2} = \frac{6gqNmc^2 r_o}{\gamma^2} \frac{\ell}{a(a+b\ell)}$$

with the numerical value of 1.94 MeV for the present case. In the table 10 parameters of bunch compression are listed.

The final focus element consists of the quadrupole double for producing the beam spot size of 2 mmϕ on the target. Bore diameter 2a of the Q magnet should satisfy the following condition,

$$\varepsilon < \frac{a}{R} r_t$$

where ε is a beam emittance, R is a stand-off distance and r_t is a beam spot radius on the target. In the present case, $\pi\varepsilon$ is 55 π (mm·mrad), r_t = 1 mm and R is 100 cm which might be too short for the reactor experiments but is enough for the beam-target experiments. The bore diameter 2a should be larger than 11.0 cm from the above relation and is designed as 20 cm. The field gradient B' and the length of the quadrupole magnet are 2.05 (kG/cm) and 1.0 m, respectively and the magnetic field strength at the pole edge is 20.5 kG which is well attainable with the super conducting magnet.

The number of beam line is supposed as two which is large enough even the space charge repulsion force is considered. Energy and power deposition on the target are expected to be 1.00 (MJ/g) and 16.4 (TW/cm^2) for the target matter of range 0.50 (g/cm^2).

3-5. Beam Instability in the Synchrotron Rings

a) Incoherent space charge limit

The xenon beam accelerated up to 5 MeV/u is to be accumulated in the first synchrotron up to its space charge limit by the multiturn injection. This limit is geven by the Laslett's formula. In the present case, this limit is calculated at 1×10^{12} for the first ring.

In the second synchrotron, the intensity of xenon beam is increased up to 1×10^{13} by the use of an RF stacking which is larger than the space charge limit of 2.5×10^{12} in the second synchrotron. In this procedure, however, the injection cycle from the first synchrotron is about 3 Hz and the tune shift due to space charge force in the second ring can be well compensated by adjusting quadrupole magnets during the cycle time of the first synchrotron.

b) Longitudinal coherent instability

Intensity limit of the longitudinal instability is given by Keil-Schnell criterion.

In the present case, the injection energy to the first synchrotron is 5 MeV/u and the fractional momentum spread is estimated at 3×10^{-3}, then the limiting current from the longitudinal instability is calculated at 72 particle mA, which is much larger compared with the circulating current in the first synchrotron (22 particle mA).

In the second synchrotron, the stability limit of the longitudinal instability is much larger ($\sim$ 5 particle A) compared with the circulating current ($\sim$ 0.7 particle A) after RF stacking because of larger momentum spread, but for the beam in the second ring at the early stage

of stacking, the momentum spread is rather small because of adiabatic damping through the acceleration process in the first ring and the stability limit is comparable with the circulating current. This situation might provide us a very interesting possibility of beam dynamics study of HIF drivers.

c) Transverse coherent instability

When the chromaticity is chosen as - 10, the transverse instability limiting current, is 4.25 particle mA and 44.8 particle mA while the circulating current is 22 particle mA and 712 particle mA for the first and second synchrotrons, respectively. The circulating current is much higher than the stability limit for both cases and this instability is anticipated to be induced. The growth rate of the instability is estimated at 50 ms and 3 ms for the first and second synchrotrons, respectively, which is rather shorter compared with the time necessary for the present experiment. However, this instability is to be surmounted by the use of a feed back damping.

d) Beam life due to interaction between beam and residual gases

For the case of heavy ions, the dominating interaction between beam and residual gases is charge exchange process. The main component of the residual gas is considered to be H_2 at ultra-high vaccum and the stripping cross section of Xe^{8+} with the residual hydrogen molecule is known to be 7.08×10^{-18} cm^2 at 28.48 Mev/u. In order to realize the beam life of 5 sec., the required vacuum pressure is 1.1×10^{-10} Torr which is well in the present art of technology.

e) Beam life due to beam-beam scattering

The cross section of the beam-beam scattering of xenon is calculated at 1×10^{-18} cm^2. For the present case the beam life due to this process is estimated to be 1.11×10^3 sec., which is long enough for the time necessary for the present experiment.

4. Conclusions

Based on the results described in section 2 and the studies on designing the NUMTATRON, the conceptual design of HIF systems are being made in Japan. Further studies with TARN and LITL will give us important results on the beam dynamics in the storage ring and low velocity RFQ linac. The NUMATRON will be more powerfulefacilities for the HIF accelerator and it will be possible to perform the tenth kJ target physics with this machine.

Acknowledgment.

The authors would like to express their thanks to the member of Numatron accelerator group at INS for their collaboration on this work. In connection with the Heavy Ion Fusion Program, Drs. T. Yamaki and H. Ohbayashi (Nagoya Univ.) are greatly acknowledged for their useful discussions.

The authours are also indebted to Profs. K. Sugimoto, M. Sakai and S. Hayakawa for their continuous encouragements.

Figure Captions

Fig. 1 Over all view of TARN

Fig. 2 Layout of TARN and SF cyclotron

Fig. 3 Multi-turn injected beam detected with electro-static monitor.

Fig. 4 Beam profiles of Multi-turn injected beam (top) and the beam which is moved to the top of stack region by the sweep of RF frequency (bottom).

Fig. 5 Intensity of stored current is measured with permalloy monitor and scintillation monitor. Intensity increases linearly up to the stacking number of 15.

Fig. 6 Beam profiles of RF stacked beam. Each number in the profile gives the number of RF stackings.

Fig. 7 RF frequency (top) and amplitude (bottom) modulations which are used for RF stacking. Horizontal scales are 5 ms/diu (a) and 1 ms /div (b), respectively.

Fig. 8 Possible working lines. A and B represent those of ideal and real magnet systems. Other lines (L∿R) represent the lines with sextupole corrections.

Fig. 9 Signals of lost beam are observed by scintillation monitors located inside the vacuum chamber. The lower shows the RF frequency variation. The plateau corresponds to the $2^1/_3$ resonances.

Fig. 10 Schottky signals observed at TARN. Two longitudinal signals corresponds to the harmonic number of 72 and 73, respectively. Signals are performed with 2500 times averaging.

Fig. 11 Observed spectrum of a longitudinal and two transverse signals. The frequency spacing Δf between the transverse and longitudinal signals is 278 kHz, while the frequency of longitudinal one is 32.882 MHz (harmonic number 29).

Fig. 12 The layout of Numatron HIF version.

Fig. 13 Parameters of linac systems.

References

1) S. Hayakawa et al., "Present Status of Heavy Ion Fusion Study in Japan", Proc. of IAEA Technical Committee and Workshop Fusion Reactor Design and Technology, 1981

2) Y. Hirao, "Present Status of Heavy-Ion Fusion Study in Japan", to this symposium.

3) Proc. of Symposium on Inertial Fusion with Heavy Ion Beams, INS-NUMA-28, 1981

4) Y. Hirao et al., "Test Accumulation Ring for NUMATRON Project", IEEE. Trans. NS Vol. NS-26, No 3 (1979)

5) T. Katayama, T. Nakanishi and S. Yamada, "Injection and Accumulation Method in the TARN", IEEE Trans. NS Vol. NS-28, No. 3 (1981)

6) A. Noda et al., "Characteristics of Magnetic Focusing and Chromaticity Correction System for TARN", ibid in reference 5)

7) D. Möhl "Longitudinal Beam Instability in Heavy Ion Storage Rings" Proc. of the Heavy Ion Fusion Workshop LBL-10301, SLAC-PUB-2575 (1979)

8) N. Ueda et al., "RF Field Measurement and its Analysis on a Model Resonator of the inter-Digital H type Linac", IEEE Trans. NS Vol. NS-28, No. 3 (1981)

9) T. Fukushima et al., "Measurement of Model Inter-Digital H Type Linac", Proc. of the 1981 LINAC Conference, LA-9234-C (1981)

Table 1 TARN Parameters

Max Beam Energy (ε = 0.3)	8 MeV/u
Max Magnetic Field	9.0 kG
Radius of Curvature	1.333 m
Average Radius	5.06 m
Useful Aperture	45 × 190 mm^2
Revolution Frequency	1.3 MHz
Betatron ν Values (ν_x, ν_z)	2 ∿ 2.5
Transition	1.894
Injection Method	Multiturn
Momentum Spread of the Stacked Beam	2.46 %
Repetition Rate of RF Stacking	33 Hz
Vacuum Pressure	1×10^{-10} Torr
Space Charge Limit (N^{5+})	6×10^{10}

Table 2 RF Voltage and Frequency Parameters

Region	I	II	III	IV
Voltage V (Volt)	0 → 77	77 → 224	224	224 → 77
Frequency Shift Δf (KHz)	0	13.7	166	120
Synchronous Phase ϕ (Degree)	0	0 → 15	15	15 → 0
Time Derivative of RF Frequency shift $\Delta f/\Delta t$ (MHz/sec)	0	0 → 27.06	27.06	27.06 → 0
Period τ (ms)	0.5	1.0	6.0	8.8
Fractional Momentum Change $\Delta p/p$ (%)	0	0.24	3.21	5.35
Change of Closed Orbit ΔR (cm)	0	0.37	4.86	8.10
Fractional Frequency Change $\frac{\Delta f}{f}$ (%)	0	0.17	2.25	3.75

$$\eta = \frac{1}{\gamma_t^2} - \frac{1}{\gamma^2} = 0.70$$

$$\frac{df}{dx} = 3.7 \text{ kHz/mm}$$

Table 3 Bunch Compression in TARN

Particle	P, 5 MeV
Number of particles	5×10^{11}
Initial bunch width	877 ns
Final bunch width	88 ns
Longitudinal beam impedance	$-j$ (3000) Ω
Inductance	$-j$ (4×10^{-4}) H
Space charge compensation	± 26.8 KV
Bunch rotation voltage ($\Delta p/p = 1 \times 10^{-2}$)	± 2.8 KV

Table 4 Comparison of Parameters related to Longitudinal Instability

	CPS	TARN	HIF
R(m)	100	5	100
β	1	0.1	0.3
γ	20	1	1
I(A)	1	0.1	60
frev (KHz)	475	1260	140
$\beta^2\gamma m_o c^2 A/q$ (Gev)	20	0.01	20
$\tilde{\eta} = \gamma_t^{-2} - \gamma^{-2}$	1/38	-0.7	-1
h(mm)	35	30	40
$n_c = R/h$	6×10^4	170	2500
$\frac{377}{\beta\gamma^2}(\frac{1}{2} + \ln\frac{b}{h})(\Omega)$	1	5500	1500
wall impedance			
$\frac{Rn}{n}(\Omega)$	2-15	2-15	2-15
$\frac{X_n}{n}(\Omega)$	20	<< 5500	<< 1500

Notations are same in the paper by D. Möhl in the proceedings of HIF workshop, 1979.

Table 5 Properties of the output Xe^{8+} beam

ion	Xe^{8+}
energy	10 GeV
	75 MeV/u
number of ions in a beam pulse	1×10^{13}
energy in a beam pulse	15.5 kJ
peak power	0.516 TW
pulse width	± 15 ns
peak current	53.3 particle A
energy deposition*	10 MJ/g
	16.4 TW/cm^2
beam size	2 mm ϕ

*The range of a 10 GeV Xe^{8+} is 0.50 g/cm^2.

Table 6 Operation conditions of the ion source and the preaccelerator

type of the source		PDPE
ion		Xe^{1+}
current		30 mA
normalized emittance	0.2	mm·mrad
accelerating voltage		200 kV

Table 7 Parameters of the RFQ linacs

ion	Xe^{1+}
frequency	12.5 MHz
injection energy	1.89 keV/u
output energy	64.2 keV/u
average radius (constant)	19.1 mm
minimum aperture	13.8 mm
synchronous phase	-90° → -30°
modulation	1 → 1.66
maximum surface field	0.15 MV/cm
overall length	28.0 m
cavity diameter	4.1 m
normalized emittance	0.2 π mm·mrad
transmission	98% (0 mA)
	83% (25 mA)

Table 8 NUMATRON Linac Specifications

	RFQ	IH1	IH2	IH3	Alvarez 1	Alvarez 2	
Operation Mode	$\pi - \pi$	$\pi - 3\pi$	$\pi - 3\pi$	$\pi - \pi$	$2\pi - 2\pi$	$2\pi - 2\pi$	
T/A (Kev/u)	1.89 - 64.2	64.2 - 150	150 - 300	300 - 1600	1600 - 5000	5000 - 10000	
Frequency (MHz)	12.5	25	25	25	100	100	
v/c (%)	0.2 ∿ 1.17	1.17 ∿ 1.77	1.77 ∿ 2.54	2.54 ∿ 5.85	5.85 ∿ 10.32	10.32 ∿ 14.55	
Particle Xe	(0.00775) Xe^{1+}	Xe^{1+}	(0.0620) Xe^{8+}	Xe^{8+}	Xe^{8+}	—	
(ε) U	(0.00840) U^{2+}	U^{2+}	U^{2+}	(0.0672) U^{16+}	U^{16+}	(0.269) U^{64+}	
Length (m)	22.4	14.16	17.85	15.32	41.25	13.28	
$\Delta T/\Delta L \cdot \varepsilon$ (MeV/m)	0.359	0.782	1.00 (U^{2+})	1.369	1.329	1.400	
Z_{eff} (MΩ/m)	7.67	89	85	145	41	35	
Power Beam	0.129	0.354	0.124	1.073	2.807	0.067 (U)	
(MW) Wall	0.228/linac	0.130	0.230	0.210	2.243	0.918 (U)	
Current Xe	16/linac	32/Funneling	6.4	6.4	6.4	—	
(pmA) U	1	1	1	0.4	0.4	0.056	
Q mag Sequence		FFDD	FFDD	FFDD	FFDD	FDFD	
G (kG/cm)		6.7 —		6.11 —	10.72 —	4.37 —	
Emittance πε	Xe 100π → 47.1π	47.1π → 45.2π	45.2π → 31.5π	31.5π → 13.7π	13.7π → 7.75π		$\pi\varepsilon_n$ (Xe)=0.2π
(mm·mrad)	U 250π → 29.4π	29.4π → 28.2π	28.2π → 19.7π	19.7π → 8.54π	8.54π → 4.84π	4.84π → 3.42π	$\pi\varepsilon_n$ (U) = 0.5π
Max Beam Size	≤13.8	Xe 21.7	21.3	17.7	11.7		
(mm)	(Min Apert.)	U 17.1	16.8	14.0	9.24	6.96	
			↑ Xe Stripper	↑ U Stripper		↑ U Stripper	

Table 9 Synchrotron Parameters

	Ring 1	Ring 2
Design Kinetic Energy (Xe^{8+})		
at injection	5 MeV/u	27.48 MeV/u
at ejection	27.48 MeV/u	75 MeV/u
Intensity	1×10^{12}	1×10^{13}
Repetition Rate	3 Hz	0.3 Hz
Radius of Curvature	10.70 m	13.75 m
Average Radius	35.65 m	40.74 m
Circumference	224.0 m	256.0 m
Focusing Structure	FODO	FODO
Number of Betatron Oscillation per Turn	6.25	6.25
Transition Energy γ_t	6.434	6.414
Number of Cell	32	32
Length of the Unit Cell	7 m	8 m
Length of the Bending Magnet	1.40 m	1.80 m
Magnetic Field of the Bending Magnet		
at injection	4.85 kG	8.91 kG
at ejection	11.45 kG	14.90 kG
Momentum Spread of the Beam		
at injection	3×10^{-3} (FW)	1.43×10^{-2} (FW)
at ejection	1.43×10^{-3} (FW)	7.0×10^{-3}
Revolution Frequency		
at injection	0.138 MHz	0.279 MHz
at ejection	0.318 MHz	0.445 MHz (2.247 μs)
Harmonic Number	7	8
Required Energy Gain per Turn	21.09 KV/Turn	28.09 KV/Turn
Vacuum Pressure	1×10^{-10} Torr	1×10^{-10} Torr

Table 10 Bunching Parameter at NUMATRON

Particle	Xe^{8+}, 10 GeV
Number of particles	1.08×10^{13}
Initial bunch width	1.124 μs
Final bunch width	112 ns
Frequency of saw tooth voltage	0.890 MHz
Longitudinal space charge impedance	$-j\,(851.9)\ \Omega$
Inductance	-3.04×10^{-4} H
Momentum spread	$\pm 3.85 \times 10^{-3} \rightarrow \pm 3.85 \times 10^{-2}$
Compensation voltage for space charge force	± 0.116 MV
Bunch rotation voltage	± 0.703 MV

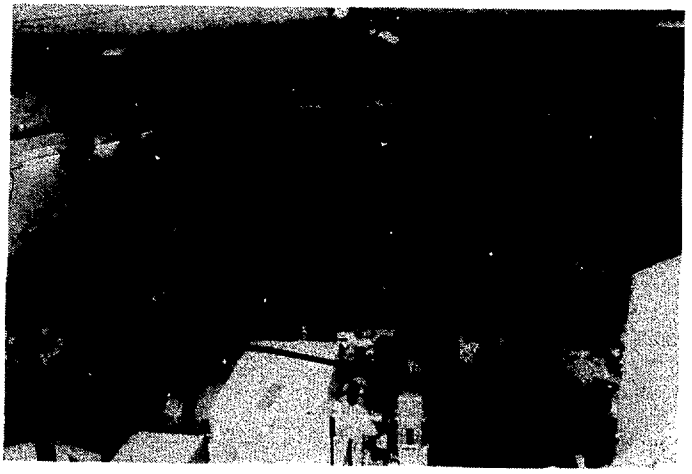

Fig. 1

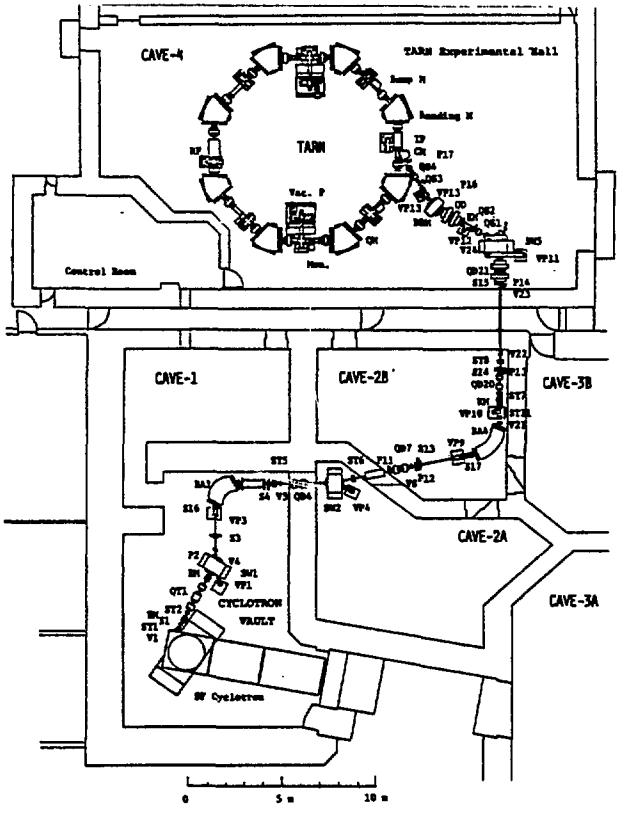
CAVE-4
TARN Experimental Hall
TARN
Control Room
CAVE-1
CAVE-2B
CAVE-3B
CAVE-2A
CAVE-3A
CYCLOTRON VAULT
SF Cyclotron
0
5 m
10 m

Fig. 2

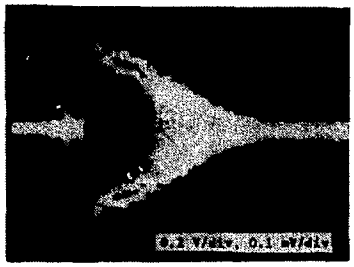

He^{++} Ion
Multiturn Injection

Fig. 3

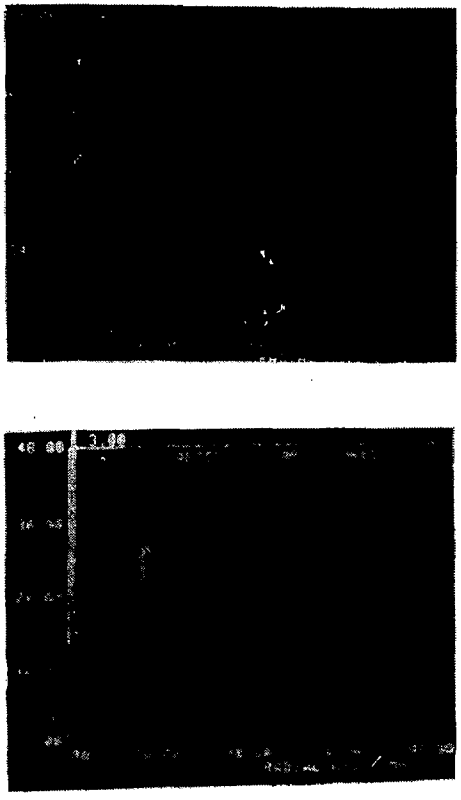

Fig. 4

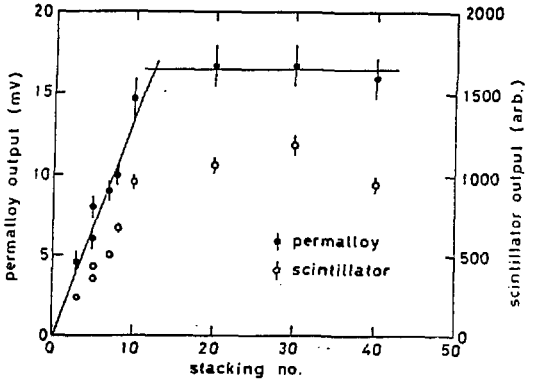
permalloy output (mV)
scintillator output (arb.)
stacking no.
permalloy
scintillator
0
5
10
15
20
500
1000
1500
2000
0
10
20
30
40
50

Fig. 5

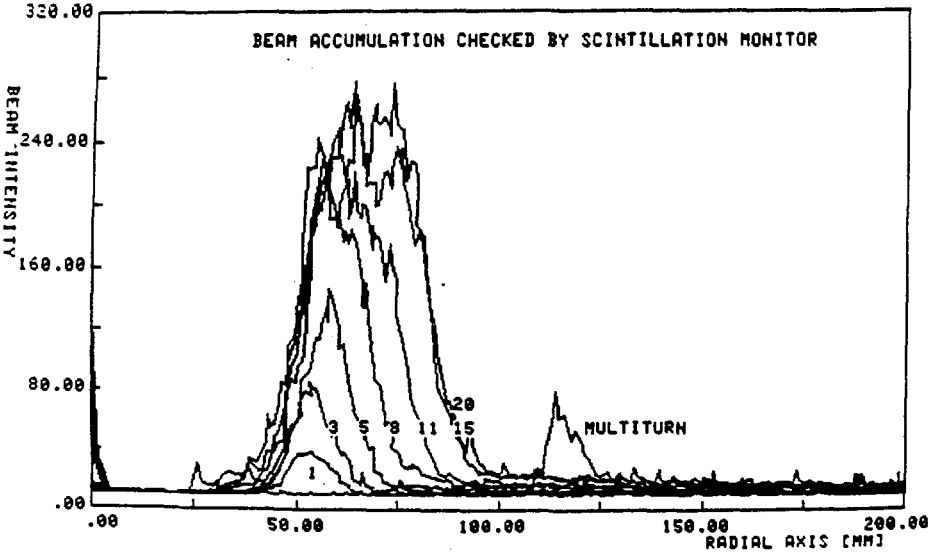
BEAM ACCUMULATION CHECKED BY SCINTILLATION MONITOR
BEAM INTENSITY
RADIAL AXIS [MM]
MULTITURN
1
3
5
8
11
15
20
320.00
240.00
160.00
80.00
.00
.00
50.00
100.00
150.00
200.00

Fig. 6

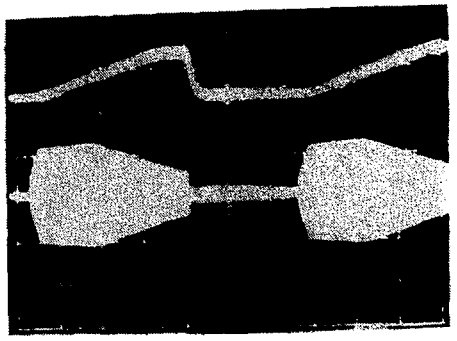

Fig. 7 (a)

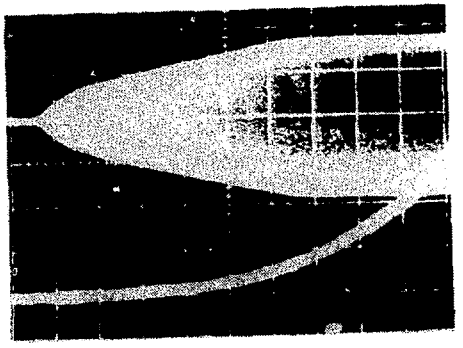

Fig. 7 (b)

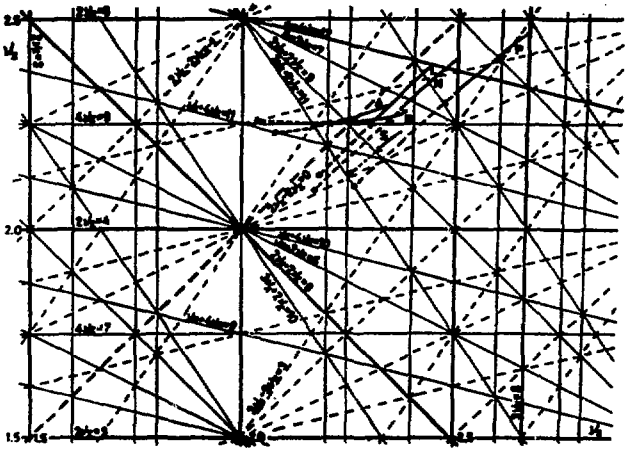

Fig. 8

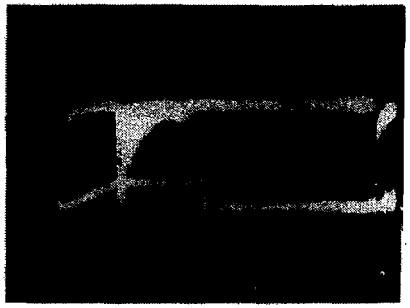

Fig. 9

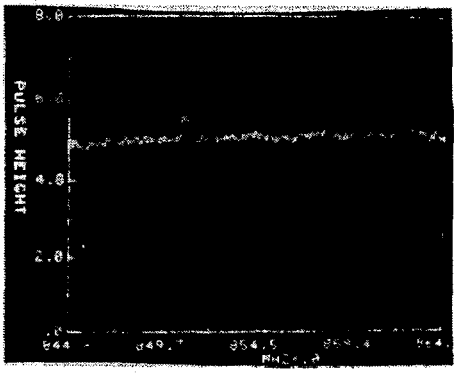

Fig. 10

Fig. 11

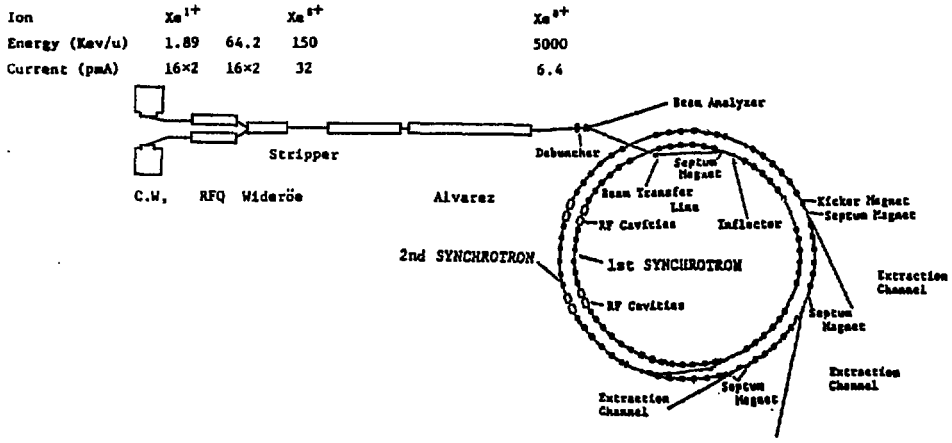
Ion
Xe1+
Xe8+
Xe8+
Energy (Kev/u)
1.89
64.2
150
5000
Current (pmA)
16×2
16×2
32
6.4
Beam Analyzer
Stripper
Debuncher
Septum Magnet
Beam Transfer Line
Kicker Magnet
Septum Magnet
RF Cavities
Inflector
2nd SYNCHROTRON
1st SYNCHROTRON
RF Cavities
Extraction Channel
Septum Magnet
Extraction Channel
Septum Magnet
Extraction Channel
C.W, RFQ Wideröe
Alvarez

Fig. 12

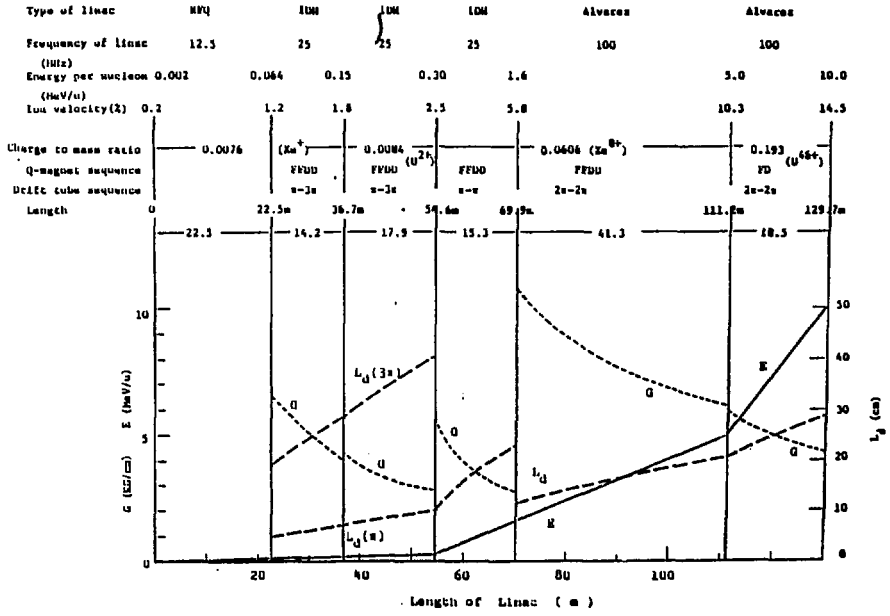
Type of linac
RFQ
IHH
IDH
IOH
Alvarez
Alvarez
Frequency of linac (MHz)
12.5
25
25
25
100
100
Energy per nucleon (MeV/u)
0.002
0.064
0.15
0.30
1.6
5.0
10.0
Ion velocity(%)
0.2
1.2
1.8
2.5
5.8
10.3
14.5
Charge to mass ratio
0.0076
(Xe+)
0.0084
(U2+)
0.0606 (Xe8+)
0.193
(U64+)
Q-magnet sequence
FFDD
FFDD
FFDD
FFDD
FD
Drift tube sequence
n-3n
n-3n
n-n
2n-2n
2n-2n
Length
0
22.5m
36.7m
54.6m
89.9m
111.8m
129.7m
22.5
14.2
17.9
15.3
41.3
18.5
G (KG/cm)
E (MeV/u)
L_d(3n)
L_d(n)
L_d
Q
E
L_q (cm)
Length of Linac (m)

Fig. 13